

Retrospective co-RASOR reconstruction and post-processing enable efficient and accurate localization of objects and devices

Hendrik de Leeuw¹, Peter R Seevinck¹, and Chris J.G. Bakker¹

¹Image Sciences Institute, Utrecht, Netherlands

Introduction: Accurate localization of field perturbing objects, such as needles, catheters and brachytherapy seeds, is a desirable feature for planning, guidance and evaluation of interventional procedures [1, 2]. Performing this task with MRI is difficult, since the signal voids generated by such devices are non-specific and distorted [3, 4]. MR data acquisition using center-out Radial Sampling with Off-Resonance reception (co-RASOR) has been shown to largely solve the mis-positioning artifact and to provide high signal in the center of field perturbers [5]. In co-RASOR a frequency offset is applied during signal reception in a center-out radial acquisition. Multiple frequency offsets are applied to determine the optimal frequency offset i.e. the offset at which the highest positive contrast is generated in the geometrical center of a field perturber [5]. Evidently, the co-RASOR method with multiple acquisitions is inefficient and hence unsuitable for near-real time interventional purposes. In this work the limitations with regard to efficiency are resolved by off-resonance reconstruction instead of off-resonance acquisition, using a single on-resonance acquired dataset. Subsequently, the images generated at multiple frequency offsets are exploited to automatically extract the frequency offset for optimal localization of the object. The accuracy will be demonstrated by comparing co-RASOR to CT for a phantom. The potential is shown using an MR compatible biopsy needle in an inhomogeneous piece of porcine tissue.

Materials & Methods: Signal pile-up around magnetic field perturbers, resulting from data acquisition by a center-out radial read-out, can be shifted and eventually focused into the center of an object, by applying a frequency offset [5]. Here this frequency offset is applied via reconstruction, by using a phase ramp in k-space for each frequency offset [6]. After reconstruction with multiple frequency offsets, an algorithm is applied to select the optimal frequency offset, at which high signal intensity is obtained in the center of an object. A schematic depiction of the algorithm is shown in Figure 1. Phantom A consisted of a 17.4mM Holmium(III)-doped agarose gel (2%), with a volume susceptibility of 0.3ppm [7] in which 2 glass spheres were placed (diameter 1.4mm, 0.8mm). Phantom B consisted of an inhomogeneous piece of porcine tissue containing fat, connective tissue and bone in which a biopsy needle (18G Coax Needle, Invivo, Schwerin, Germany) was inserted. Phantom B was oriented in three directions (0, 45° and 90° w.r.t. B_0) to mimic image artifacts as obtained during interventions.

Phantom A was subjected to a CT scan, with voltage 140KV, mAs 250, in-plane resolution 0.67mm and increment 0.33mm. MR imaging was done on a 1.5T whole body MR scanner (Achieva; Philips Healthcare, Best, The Netherlands) using a birdcage head coil. A 3D FID with center-out radial read-out was acquired. Scan parameters included a volume excitation by a hard, non selective, RF block pulse (BW = 26kHz), field of view (FOV) 128^3 mm 3 , matrix 128^3 , echo time (TE) 0.15ms, repetition time (TR) 4.7ms, flip angle (θ) 15° and read-out BW 868Hz/pixel, resulting in a scan duration of 2.34 min for phantom A. Scan parameters for phantom B included same RF-pulse, FOV 176^3 mm 3 , matrix 176^3 , TE 0.15ms, TR 5.5ms, θ 15°, read-out BW 887Hz/voxel and scan duration 5.39 min. Post-processing was done using Matlab (The MathWorks, Inc, Natick, MA). Reconstruction of a 128^3 dataset required 2 sec, localization of the maxima less than 1 sec. CT and co-RASOR images of phantom A were rigidly registered.

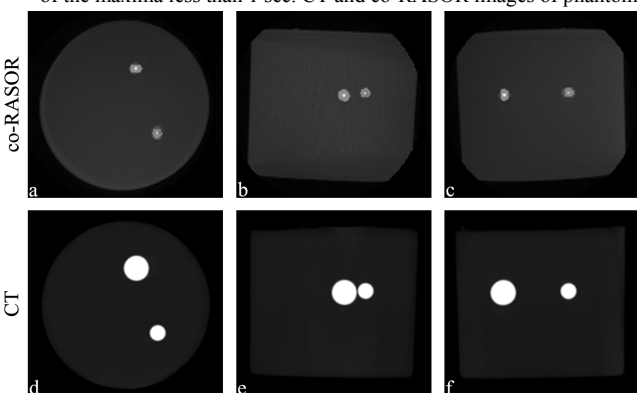


Figure 2: Maximum intensity projection (MIP) of co-RASOR (top) and CT (bottom) along the sagittal (c,f), transverse (a,d) and coronal (b,e) direction.

Discussion: In this work the positive contrast in the geometric center of a field perturber, as achieved by selecting the optimum from multiple acquisitions in previous work [5], is obtained by performing multiple off-resonance reconstructions. Because of the post-processing nature, the efficiency and flexibility of co-RASOR was increased, as shown in Figure 3. Using the reconstructions, the center of the perturber is located automatically. Background suppression is obtained via thresholding. The accuracy of co-RASOR resembles that of CT (Figure 2). Unlike in CT, the high signal intensity for co-RASOR is no absolute quantity, but determined by the strength of the perturber, the voxel size and the read-out gradient strength. In contrast to de-blur methods [6], a global magnetic field offset is applied to over-compensate signal pile-up, resulting in high signal in the center of the field perturber [5]. Figure 3 illustrates the applicability to inhomogeneous structures. Because of the fast and accurate depiction of field disturbances and the high positive contrast, co-RASOR is useful for position verification. Using these perspectives and our current results, we expect co-RASOR post-processing to develop into a valuable clinical and research tool.

References: [1] F.K. Wacker et al. *Radiology*, 238(2):497–504, 2006. [2] C. Perlet et al. *European Radiology*, 12(6):1463–1470, 2002. [3] M.A. Moerland et al. *PMB*, 40(10):1651–1664, 1995. [4] Reichenbach, J.R. et al. *JMRI*, 7:266–279, 1997. [5] P.R. Seevinck et al. *MRM*, 65:146–156, 2011. [6] H. Schomberg. *IEEE TMI*, 18(6):481–495, 1999. [7] C.J.G. Bakker et al. *MRM*, 56(5):1107–1113, 2006. [8] E.M. Haacke et al. John Wiley and Sons, Inc., 1999.

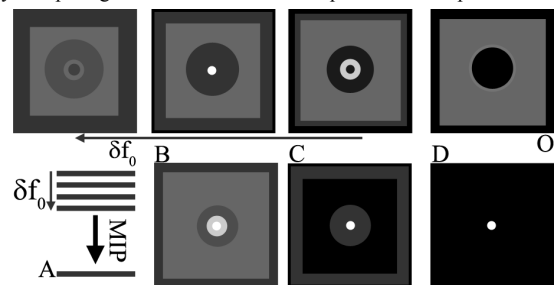


Figure 1: Schematic depiction of the algorithm. First, the acquired image (image O) is reconstructed at a number of frequency offsets. Subsequently, voxelwise the maximum signal intensity as function of the offset is determined (image A). Thereafter, the reconstruction corresponding to the maximum signal intensity in image A is selected (image B). Background is suppressed by subtracting the in on-resonance acquired image (image C) and subsequently thresholding (average + 3 × standard deviation of the signal intensity, image D). The process is iterated and stops when image A^{N+1} ($=A^N - D^N$, with $N \geq 0$, # iterations) is below threshold. After post-processing image O and the positive contrast are fused.

Results: Figure 2 shows the comparison of co-RASOR to CT, after rigid registration of both modalities. Figure 2 shows a close correspondence for CT and co-RASOR. Small differences can be attributed to differences in resolution, contrast and post-processing. The location of the signal maxima of the two spheres on co-RASOR MRI correspond well with the location of the centers of the spheres on CT, with nearly equal Pythagorean distances between the two spheres (left column: 44.4mm co-RASOR, 44.3mm CT; middle column 14.1mm co-RASOR, 14.0mm CT; right column 42.4mm co-RASOR, 42mm CT).

Figure 3 shows the piece of porcine tissue with three orientations with respect to B_0 . The three needle orientations were found to require three different frequency offsets for optimal depiction (1.25 kHz (a), 2.25 kHz (b) 2.75 kHz (c)). Because of the relatively short TR used during the experiments, the signal of fat is high in Figure 3. The needle parallel to B_0 shows little signal in the needle except at the tip after co-RASOR reconstruction (Figure 3d), since the field disturbance of a cylinder about parallel to B_0 is small along the cylinder, but large at the tip [8]. The signal intensity at the tip of the needle is clearly highest, for all needle orientations.

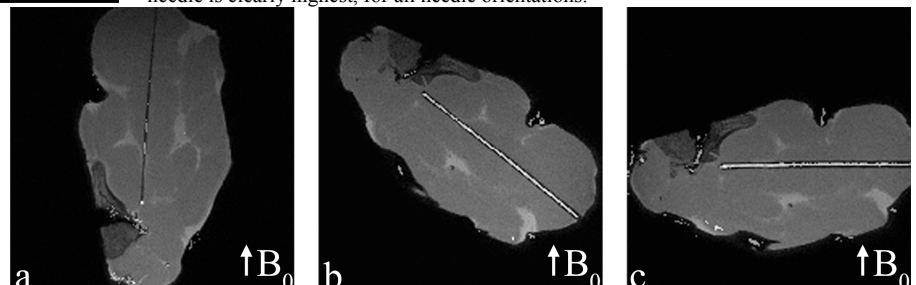


Figure 3: MIP of the co-RASOR of the needle in porcine tissue. Three needle orientations were applied to show the flexibility of the technique and the need for it. Arrows indicate the direction of B_0 .